Earth Syst. Dynam., 12, 621–634, 2021
https://doi.org/10.5194/esd-12-621-2021
© Author(s) 2021. This work is distributed under
the Creative Commons Attribution 4.0 License.

Earth System Dynamics
Open Access
EGU

Space–time dependence of compound hot–dry events in the United States: assessment using a multi-site multi-variable weather generator

Manuela I. Brunner, Eric Gilleland, and Andrew W. Wood

Research Applications Laboratory, National Center for Atmospheric Research,
3450 Mitchell Ln, Boulder, CO 80301, USA

Correspondence: Manuela I. Brunner (manuela.brunner@hydrology.uni-freiburg.de)
and Eric Gilleland (ericg@ucar.edu)

Received: 10 February 2021 – Discussion started: 11 February 2021
Revised: 13 April 2021 – Accepted: 22 April 2021 – Published: 19 May 2021

Abstract. Compound hot and dry events can lead to severe impacts whose severity may depend on their timescale and spatial extent. Despite their potential importance, the climatological characteristics of these joint events have received little attention regardless of growing interest in climate change impacts on compound events. Here, we ask how event timescale relates to (1) spatial patterns of compound hot–dry events in the United States, (2) the spatial extent of compound hot–dry events, and (3) the importance of temperature and precipitation as drivers of compound events. To study such rare spatial and multivariate events, we introduce a multi-site multi-variable weather generator (PRSim.weather), which enables generation of a large number of spatial multivariate hot–dry events. We show that the stochastic model realistically simulates distributional and temporal autocorrelation characteristics of temperature and precipitation at single sites, dependencies between the two variables, spatial correlation patterns, and spatial heat and meteorological drought indicators and their co-occurrence probabilities. The results of our compound event analysis demonstrate that (1) the northwestern and southeastern United States are most susceptible to compound hot–dry events independent of timescale, and susceptibility decreases with increasing timescale; (2) the spatial extent and timescale of compound events are strongly related to sub-seasonal events (1–3 months) showing the largest spatial extents; and (3) the importance of temperature and precipitation as drivers of compound events varies with timescale, with temperature being most important at short and precipitation at seasonal timescales. We conclude that timescale is an important factor to be considered in compound event assessments and suggest that climate change impact assessments should consider several timescales instead of a single timescale when looking at future changes in compound event characteristics. The largest future changes may be expected for short compound events because of their strong relation to temperature.

1 Introduction

Compound hot and dry events, i.e., events that are extreme with respect to both temperature and precipitation, can lead to severe impacts on agriculture and other sectors as illustrated by the 2010 heatwave–drought in Russia and the 2012 heatwave–drought in the central United States (US; Mo and Lettenmaier, 2015), which led to substantial reductions in crop yields (Wegren, 2011; Christian et al., 2020; Fuchs et al., 2012). The US has been shown to be affected by concurrent hot and dry events at different timescales including short and long events effective at weekly to monthly (Zhang et al., 2020) and seasonal to annual timescales (Alizadeh et al., 2020), respectively. The interest in these impactful compound events is reflected in an increasing number of studies assessing changes in their frequency of occurrence. Substantial increases in the number of concurrent droughts and heatwaves over the last few decades that are

partly explained by increasing temperatures have been reported not just for the US (Alizadeh et al., 2020; Mazdiyasni and AghaKouchak, 2015; Tavakol et al., 2020) but also globally (Feng et al., 2020; Sarhadi et al., 2018) and for other regions of the world such as China (Wu et al., 2019; Zhou and Liu, 2018; Yu and Zhai, 2020) and Europe (Manning et al., 2019).

While frequency of occurrence is an important factor determining impacts, the severity of impacts related to compound events likely also depends on their spatial extent, i.e., how large the affected region is, and their timescale, i.e., whether they just last weeks or extend over a longer period of time. Indeed, spatiotemporal behavior is a common target of analyses in general for drought, a related phenomenon, as in the multi-temporal severity-area-duration analyses presented by Andreadis et al. (2005). Despite their potential importance for understanding and projecting the physical manifestation and impacts of compound events, these spatiotemporal characteristics have received comparably little attention. Only recently have Alizadeh et al. (2020) and Wu et al. (2021) shown that the area affected by concurrent hot–dry extremes has increased significantly over the past few decades in the US and globally for long, i.e., seasonal, timescales. However, it remains to be investigated how the timescale of compound events influences their characteristics and spatial extent.

This study aims to deepen our understanding of how the timescale of compound hot–dry events in the US relates to (1) spatial patterns of compound event affectedness (i.e., where in the US hot–dry events are most frequent), (2) spatial extents of compound events (i.e., how large compound events are), and (3) the role of temperature and precipitation as drivers of compound events by focusing on multivariate and spatial extreme events (Zscheischler et al., 2020). To answer the question of how timescale shapes compound event characteristics, we determine the probability, extent, and drivers of spatial multivariate heatwaves and meteorological drought over the conterminous US (CONUS) for different timescales ranging from weekly to annual events.

Studying such spatial multivariate events is challenging because they are rare in observational records (Zscheischler et al., 2018). This challenge can, for example, be tackled by developing stochastic simulation approaches to generate large data sets with similar statistical properties as the observations (Vogel and Stedinger, 1988). A stochastic approach to simulate spatial multivariate hot–dry events at different timescales needs to (1) represent spatial dependencies between sites to capture the spatial aspect, (2) represent dependencies between variables to capture dependencies between precipitation and temperature, and (3) be continuous to enable studying timescales from weeks to years. However, existing models often only fulfill one or two of these three requirements. On the one hand, existing spatial models for simulating spatial extreme events, such as the conditional exceedance model by Heffernan and Tawn (2004), are event-based (Keef et al., 2013; Diederen et al., 2019) and often applied to one variable, e.g., flood peaks. On the other hand, continuous stochastic approaches, such as autoregressive moving-average-type models (Stedinger and Taylor, 1982) or bootstrap approaches (Rajagopalan et al., 2010), do not represent spatial dependencies well. Therefore, Brunner and Gilleland (2020) recently proposed a novel stochastic approach for simulating continuous streamflow time series in multiple catchments based on the wavelet transform. The Phase Randomization Simulation using wavelets (PRSim.wave) model combines an empirical spatiotemporal model based on the wavelet transform and phase randomization with the flexible four-parameter kappa distribution and builds on an earlier univariate version of the model (PRSim; Brunner et al., 2019). It is able to simulate continuous, spatially consistent time series but has so far only been applied to one variable (streamflow).

We extend PRSim.wave here to multiple variables by proposing a multi-site multi-variable stochastic weather generator (PRSim.weather) that simulates long time series of spatially consistent temperature (T) and precipitation (P) time series. This multi-site multi-variable stochastic model reproduces local variable distributions using flexible distributions for T and P and introduces spatiotemporal and variable dependence using the wavelet transform (Torrence and Compo, 1998) and phase randomization (Schreiber and Schmitz, 2000; Lancaster et al., 2018). Using this multi-site multi-variable generator to simulate a large set of spatial multivariate hot–dry events will help to shed light on the question of how timescale shapes compound event characteristics including spatial extent. Thus, this analysis will provide crucial information to increase preparedness and develop adaptation measures for potentially impactful spatial multivariate events.

2 Methods and materials

We develop a multi-variable multi-site weather generator that stochastically simulates spatially consistent daily T and P time series for a large number of locations. We apply this model to a gridded T and P data set in the CONUS to generate a large sample of spatial multivariate hot–dry events. We subsequently use this sample to determine which regions in the US are susceptible to compound events and large spatial multivariate event extents at different timescales. Last, we look at how the importance of T and P for compound event development varies with timescale.

2.1 Study region and data

The analysis is performed using a gridded data set of daily T and P time series for 894 equally spaced grid cells in the CONUS. T and P data were obtained from the ERA5-Land reanalysis for the period 1981–2018 (ECMWF, 2019). ERA5-Land relies on atmospheric forcing from the ERA5 reanalysis (Hersbach et al., 2020) and provides variables at

a spatial resolution of 9 km for the period of 1981 to the present. We chose a subset of regularly spaced grid cells by sampling 1500 grid cells over the extent of the CONUS, which resulted in 894 grid cells over land that are used for this analysis.

2.2 Methods

2.2.1 Stochastic multi-site multi-variable modeling

To study compound hot–dry events, we develop a multi-site multi-variable weather generator, PRSim.weather, that enables simulation of large sets of spatially consistent compound hot–dry events at a daily scale. PRSim.weather combines an empirical spatiotemporal model based on the wavelet transform and phase randomization with two flexible parametric distributions for T and P, which enables extrapolation to yet unobserved values. It builds on the spatial stochastic model PRSim.wave (Phase Randomization Simulation using wavelets) proposed by Brunner and Gilleland (2020), which simulates continuous streamflow time series at multiple sites. We expand the functionality of PRSim.wave to simulate multiple variables, i.e., T and P, at multiple sites. The weather generation procedure implemented in PRSim.weather consists of five main steps (Fig. 1).

1. Feed in observed daily T and P time series for multiple sites (here grid cells).

2. Fit monthly distributions to T and P time series at each site to capture seasonal variations in distribution parameters (i.e., one separate distribution is fitted to the data in each month). Using theoretical instead of empirical distributions will allow us to generate extreme values more extreme than the observations. For T, we use the flexible skewed exponential power (SEP) distribution with four parameters (Fernández and Steel, 1998), which generalizes the Gaussian distribution, can reproduce different skewness and kurtosis, and has been previously applied for multi-site temperature simulation (Evin et al., 2019). The SEP distribution is defined as

$$F(x) = \begin{cases} [\kappa^2/(1+\kappa^2)]\gamma\{[(\xi - x)/(\alpha\kappa)]^h, 1/h\} & \text{for } x < \xi \\ 1 - [1/(1+\kappa^2)]\gamma\{[\kappa(x-\xi)/\alpha]^h, 1/h\} & \text{for } x \geq \xi \end{cases}, \quad (1)$$

   with location parameter ξ, scale parameter α, shape parameters κ and h, and $\gamma(Z, \alpha)$ representing the upper tail of the incomplete gamma function (Asquith, 2014).

   The parameters of the SEP distribution are estimated using L-moments (R package lmomco; Asquith, 2020). For P, we use an extended generalized Pareto distribution (E-GPD; Papastathopoulos and Tawn, 2013) with three parameters to model positive precipitation values. The E-GPD jointly models non-extreme and extreme values of P while bypassing the threshold selection problem as it enables smooth transitioning between a gamma-like distribution and a heavy-tailed generalized Pareto distribution (GPD) thanks to a transformation function $G(v)$ (Naveau et al., 2016). The E-GPD is defined as

$$F\{x\} = G[H_\theta\{x/\sigma\}],$$

$$\text{where} \quad H_\theta(z) = \begin{cases} 1 - (1+\theta z)^{-1/\theta} & \text{if } \theta \neq 0, \\ 1 - e^{-z} & \text{if } \theta = 0, \end{cases} \quad (2)$$

   where $\sigma > 0$ is a scale parameter, θ is the shape parameter of the GPD, and $G(v) = v^\rho$. The E-GPD has been demonstrated to be valuable in multi-site precipitation modeling thanks to its flexibility (Evin et al., 2018). The parameters of the E-GPD distribution are estimated using probability weighted moments (R package mev; Belzile et al., 2020). We use the E-GPD to simulate nonzero precipitation values and complement it with as many zero values as in the observations to obtain the full P distribution with an appropriate probability of precipitation occurrence.

3. Transform the T and P time series from the time to the frequency domain by decomposing the series into an amplitude and phase signal using a continuous wavelet transform with the Morlet wavelet (Torrence and Compo, 1998) (R package wavScalogram; Bolós and Benítez, 2020). The continuous wavelet transform is defined as the convolution of a time series x_n of length n:

$$W_n(l) = \sum_{n'=0}^{N-1} x_{n'} \psi_0^* \left[\frac{(n'-n)\delta t}{l} \right], \quad (3)$$

   where the (*) indicates the complex conjugate, l the wavelet scale, and $\psi_0(\eta)$ the Morlet wavelet, which is defined as

$$\psi_0(\eta) = \pi^{-1/4} e^{i\omega_0\eta} e^{-\eta^2/2}, \quad (4)$$

   where η is a nondimensional time parameter, ω_0 is the nondimensional frequency, and $i = \sqrt{-1}$ is the imaginary unit.

4. Generate one random time series using bootstrap resampling on the temperature time series of one randomly sampled site by sampling years with replacement. Use the wavelet transform to also decompose this bootstrapped series in order to obtain a random phase signal.

5. Generate stochastic time series for T and P by applying the inverse wavelet transform to the observed amplitude signals and the randomly generated phases. Rank-transform the newly generated time series using the probability integral transform to the desired distribution for each month using the monthly distribution parameters derived in Step 2 (SEP parameters for T and E-GPD parameters for P).

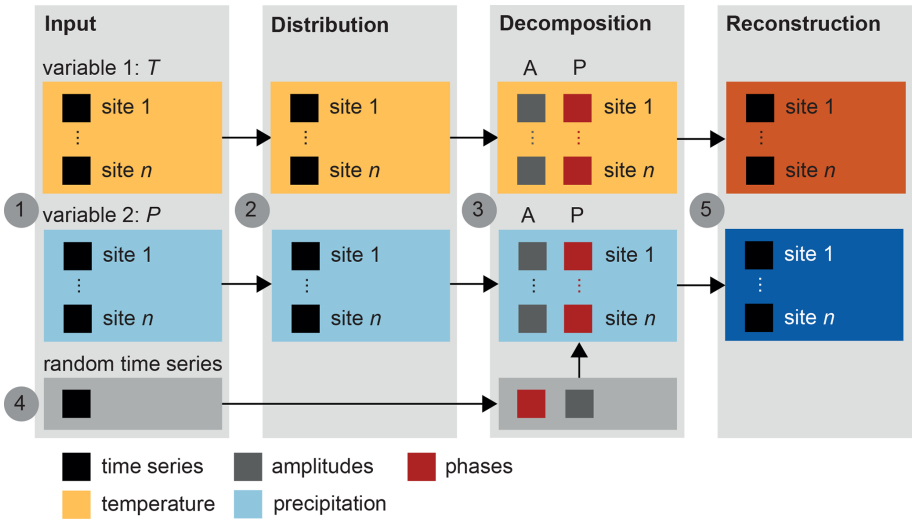

Figure 1. Illustration of the five working steps of PRSim.weather: (1) feed in daily observed temperature (T) and precipitation (P) time series for multiple sites ($1, \ldots, n$); (2) fit SEP distribution to T and E-GP distribution to P time series of all sites at a monthly scale; (3) decompose T and P time series of all sites into an amplitude (A) and phase (P) signal using the wavelet transform; (4) generate one random time series using bootstrap resampling and decompose that random series into an amplitude and phase signal too; and (5) generate random daily T and P time series by combining the observed amplitude signal of each site and variable with the randomly generated phase signal and by back-transforming the signals to the time domain using the inverse wavelet transform. Rank-transform the newly generated signal to the desired distribution using the parameter estimates from Step 2.

The simulation of yet unobserved magnitudes becomes possible thanks to the use of parametric distributions for T and P in Step 2. The spatial and variable dependencies are introduced in Step 5 by using the same random phases in the wavelet transform at all sites and for both variables.

The stochastic multi-site multi-variable model is evaluated with respect to the following characteristics: (1) T and P distributions (CDFs) at individual sites, (2) temporal autocorrelation of T and P (ACFs) at individual sites, (3) spatial dependencies across sites for T and P (variograms), (4) T–P variable dependencies (scatter plots), and (5) simulated spatial patterns of the standardized temperature index (STI), the standardized precipitation index (SPI), and the probability of compound high STI and low SPI anomalies at a 1-month aggregation level for moderate, severe, and extreme events according to the empirical copula (see Sect. 2.2.2).

PRSim.weather is finally run $n = 100$ times for the 894 grid cells in the US in order to substantially increase the sample size available for the assessment of compound hot–dry events by pooling the different model runs ($28 \text{ years} \cdot 100 = 2800$ years).

2.2.2 Compound event analysis

While the focus is on the simulated series, compound events and their corresponding T and P characteristics are identified at different timescales in both the observed and stochastically simulated time series to assess the reliability of the stochastic model. To look at different timescales, we first convert the T and P series to weekly and monthly series using mean values and sums, respectively. We work with aggregation levels of 1 week to represent "flash" compound events and of 1, 3, 6, and 12 months to represent sub-seasonal, seasonal, and annual timescales. In a second step, we transform the aggregated T and P series to series of standardized indices, which we will use to study relationships between the marginal behavior of compound events because they guarantee variable and site comparability. Standardized precipitation index (SPI) series (McKee et al., 1993) for each location are computed by transforming the P values to a standardized normal distribution (mean 0 and SD 1) using a site-specific E-GPD distribution (the Kolmogorov–Smirnov test did not reject gamma in over 80 % of the grid cells). Similarly, we compute standardized temperature index series (STI; Zscheischler et al., 2014) using the SEP distribution for transformation. Last, compound hot–dry events are identified for each timescale and grid cell using a bivariate empirical copula (Deheuvels, 1979; Genest and Favre, 2007), which describes the joint distribution of T (STI) and P (SPI) with uniform margins. We change the sign of the SPI values to convert negative to positive anomalies as we are interested in events during which STI and SPI are extreme. The empirical copula of STI and SPI is described as

$$C_n(u, v) = \frac{1}{n} \sum_{i=1}^{n} 1\left(\frac{R_i}{n+1} \leq u, \frac{S_i}{n+1} \leq v\right), \quad (5)$$

where R_i and S_i represent pairs of ranks (across STI and SPI time series), n the sample size, and $C_n(u, v)$ the rank-based

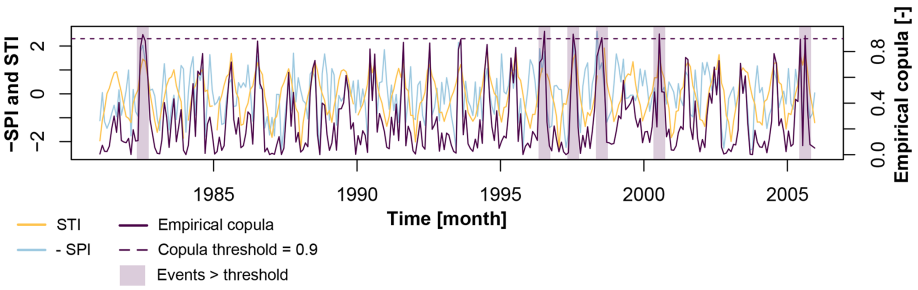

Figure 2. Illustration of the relationship between monthly STI (yellow) and SPI (blue) time series and their bivariate copula (i.e., the values of $C_n(\frac{R_i}{n+1}, \frac{S_i}{n+1})$; purple) for one example grid cell. Compound STI and SPI events exceeding a copula-threshold of 0.9 are highlighted by purple boxes.

estimator of the copula $C(u, v)$. An example of how the empirical copula (purple) is related to the margins STI (yellow) and SPI (blue) is provided in Fig. 2.

Using the time series of empirical bivariate distribution values, we identify moderate, severe, and extreme compound events using three thresholds at 0.8, 0.9, and 0.95, respectively (see Fig. 2 for an example with a threshold of 0.9). This copula-based threshold procedure slightly differs from an approach whereby both margins (SPI and STI) have to jointly exceed a threshold in order for an event to be defined as a compound event. The bivariate threshold procedure includes a slightly different event space, which besides the jointly marginally extreme events also includes those events that are extreme in terms of the bivariate distribution but not necessarily in terms of both margins. Please note that the focus on high T and low P events leads to the selection of compound events in the summer season. For an aggregation period of 1 month, all selected compound events happen between May and October, with over 90 % of the events happening in July or August. The seasonal focus is slightly shifted towards late summer (August) and early fall (September and October) as we move towards longer aggregation periods.

To assess the spatial extent of compound events at different timescales, we define the spatial extent of the compound event as the percentage of grid cells affected by the compound event at any given timescale. Then, for each grid cell, we determine the median spatial extent of those events it is affected by at each timescale.

To explain the role of the individual variables T and P in compound event occurrence, we compute Kendall's correlation between the median bivariate distribution (empirical copula) and the median standardized indices STI and SPI over all simulation runs at different timescales. This correlation analysis is performed for nine hydroclimatic regions in the United States (Bukovsky; Bukovsky, 2011) to quantify the regional spread in the role of STI and SPI for compound event development; i.e., correlation is computed between median bivariate distributions and median STI or SPI at different grid cells within a region. We look at correlations for different timescales and event extremeness levels to assess to which degree these two factors influence STI and SPI importance.

3 Results

3.1 Evaluating the weather generator

The multi-site multi-variable stochastic simulation approach in PRSim.weather is capable of reproducing the observed statistical characteristics of T and P time series at individual locations as illustrated by one example station (Fig. 3). The flexible SEP and E-GPD distributions capture the local T and P distributions well as indicated by the good match of simulated with observed densities (Fig. 3a and b). The suitability of the SEP and E-GPD distributions to model local T and P distributions also extends to the tails as 100-year return levels estimated from the observed and simulated series compare well for both variables. The temporal autocorrelation in both variables is realistically reproduced, as shown by the good agreement of simulated with observed autocorrelation functions, thanks to the observed frequency spectrum information used in the inverse wavelet transform (Fig. 3c and d). The simulated time series mimic the main temporal characteristics of the observed time series well, including seasonality and temporal event distribution and clustering as illustrated by 3 years of observed and simulated T and P data (Fig. 3e and f). The T–P variable dependence is also generally well captured thanks to the use of the same random phases for both variables when applying the inverse wavelet transform (Fig. 3g and h). However, the number of high T–low P events at a daily scale is slightly underestimated. The above-described model evaluation can be generalized to other grid cells in the data set. In addition to these local characteristics, spatial correlations are captured as illustrated by the similarity of observed and simulated variograms (Fig. 4). However, the spatial correlation of T is slightly overestimated by the simulations. Achieving a "perfect" joint representation of the three forms of dependence – temporal, spatial, and variable – is very challenging. The model is considered suitable for the analysis of compound hot–dry events

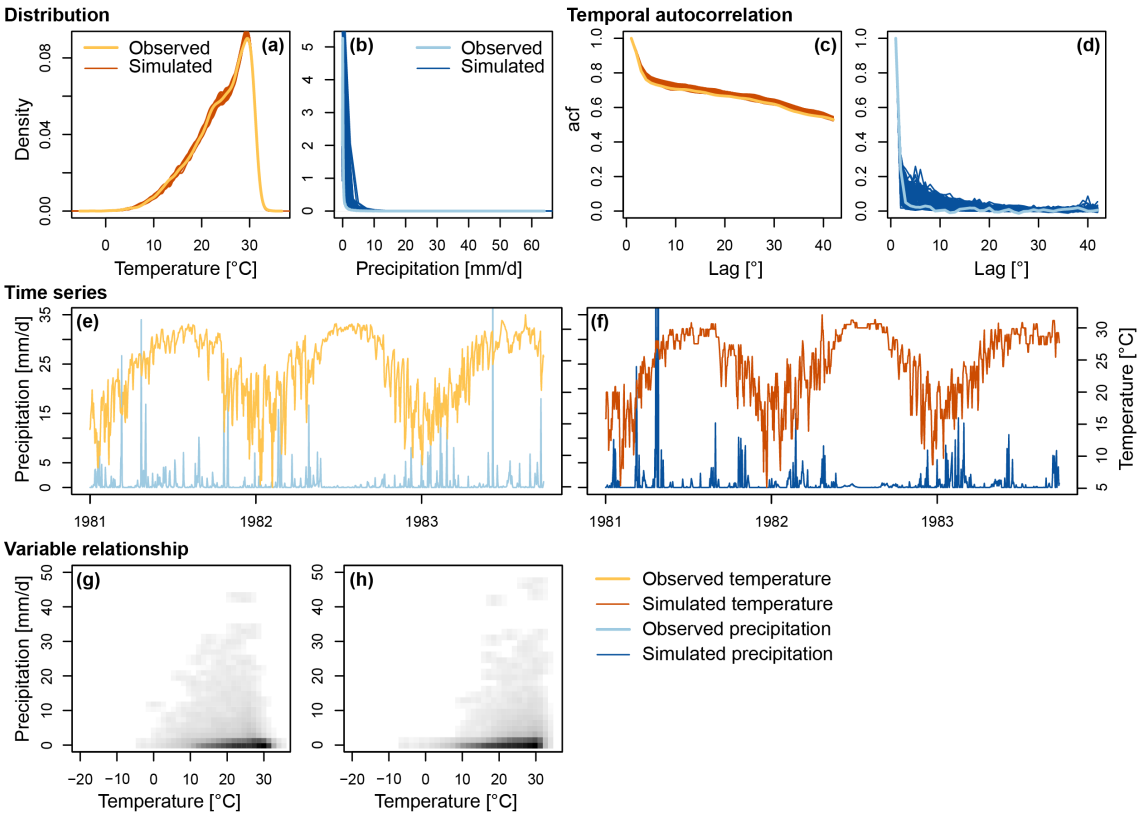

Figure 3. PRSim.weather evaluation for one example grid cell: **(a, b)** marginal distributions for observed and simulated T (orange) and P (blue) (one line represents one simulation run), **(c, d)** temporal autocorrelation for observed and simulated T and P (one line represents one simulation run), **(e, f)** 3-year time series of T (right y axis) and P (left y axis) for observations and simulations, and **(g, h)** heat scatter plot of the P–T relationship in observations and simulations.

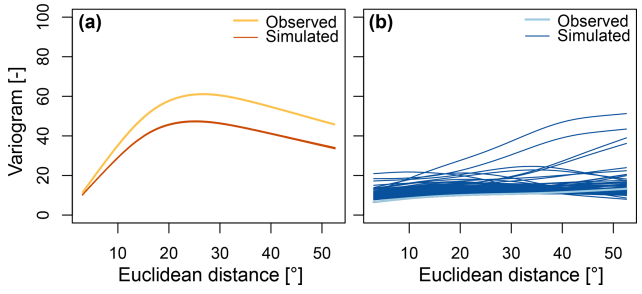

Figure 4. PRSim.weather evaluation for spatial dependence: **(a)** observed vs. simulated T (orange) variograms for 92 equally spaced grid cells and **(b)** observed vs. simulated P (blue) variograms for 92 grid cells, which describe the degree of spatial dependence of a field (Cressie, 1993).

because it has an acceptable performance with respect to all three aspects and enables increasing the sample size of compound events.

PRSim.weather enables simulation of a large sample of extreme events in terms of standardized temperature (STI) and precipitation indices (SPI). These spatial samples enable comparing observed and simulated STI and SPI patterns for different levels of extremeness (Fig. 5). While the simulated spatial STI and SPI patterns look similar to the observed ones, they are more expressed because of the larger sample available, which contains yet unobserved extremes because of the use of parametric distributions for simulating T and P. The spatial pattern for STI is rather weak, with STI values being relatively homogeneously distributed except for the Pacific Northwest and along the west coast where STI values are slightly higher than in the rest of the country. In contrast, the spatial pattern of median SPIs is expressed with substantially higher negative anomalies in the western than the eastern US and particularly strong negative anomalies in the southwest.

The spatial STI and SPI patterns are reflected in the spatial distribution of the probability of compound hot–dry events, which is also realistically represented but slightly underestimated by PRSim.weather (Fig. 6). The highest probability of compound hot–dry events at a monthly timescale is found in the Pacific Northwest, along the west coast, in the Rocky Mountains, and in the southeast, in particular in Texas. In contrast, compound hot–dry events are relatively rare in the Great Plains, the midwest, and Florida. For the remainder of

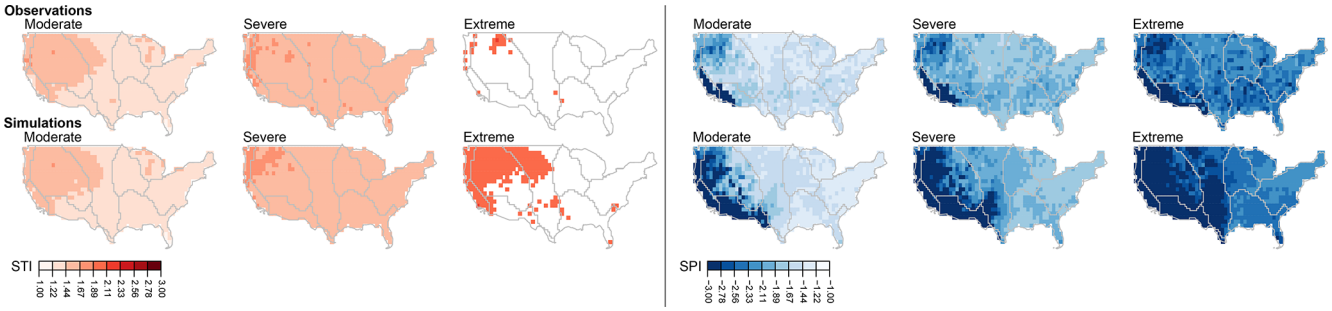

Figure 5. Spatial distribution of median observed (upper panel) and simulated (lower panel) STIs (left panel) and SPIs (right panel) at a monthly timescale for three levels of extremeness: moderate (STI > 1 and SPI < -1), severe (STI > 1.5 and SPI < -1.5), and extreme (STI > 2 and SPI < -2). The darker the color, the more severe the median events in a certain grid cell.

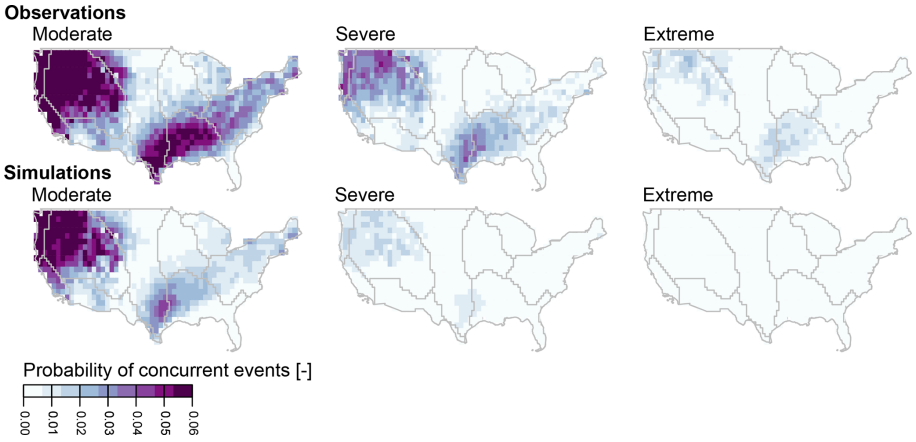

Figure 6. Spatial distribution of observed (upper panel) and simulated (lower panel) probability of occurrence of hot–dry events (number of compound events compared to the total number of months) at a monthly timescale for three levels of extremeness: moderate ($C_n > 0.8$), severe ($C_n > 0.9$), and extreme ($C_n : 0.95$). The darker the color, the more likely compound hot–dry events are.

our analysis, we focus on the stochastic simulations because of their large sample size, which allows us to study rare spatial multivariate hot–dry events.

3.2 Compound hot–dry events

The stochastically simulated compound hot–dry events reveal that the probability of co-occurring hot and dry periods is highest in the northwestern and southeastern US independently of the timescale considered (Fig. 7). However, the probability of compound events decreases with increasing duration, as can be expected due to the aggregation over increasingly longer periods of multiple weather events that may not all favor instantaneous compound hot–dry conditions and joint extremeness. Still, there are spatial nuances depending on the timescale considered. For example, the high probabilities of compound events are located in the south for short timescales and move to the southeast as we move towards longer timescales. Timescale not only affects local concurrence probabilities but also the size of the regions affected by compound hot–dry events, which decreases with increasing timescale and event extremeness. At an annual timescale, the probability of events at all extreme thresholds is negligible.

Different regions of the US differ not only in how susceptible they are to compound hot–dry event occurrence but also in how likely they are to be affected by a widespread (large spatial scale) compound event. The spatial occurrence patterns for spatially extensive compound hot–dry events vary by timescale (Fig. 8). For moderate extremes, the midwest is the most affected by large events, with more prevalence in the upper midwest at shorter timescales and the central to southern midwest at longer timescales. For the severe category, the western and southeastern regions are more affected, which is a similar spatial pattern as the probability of compound hot–dry events (Fig. 7), although there are no large-scale events at a short timescale. In addition, large compound events generally become less likely as we move beyond the 3-month timescale and toward extreme events (Fig. 9). While $\sim 20\,\%$ of the CONUS may be jointly affected by moderate and short compound events, spatial extents of compound events be-

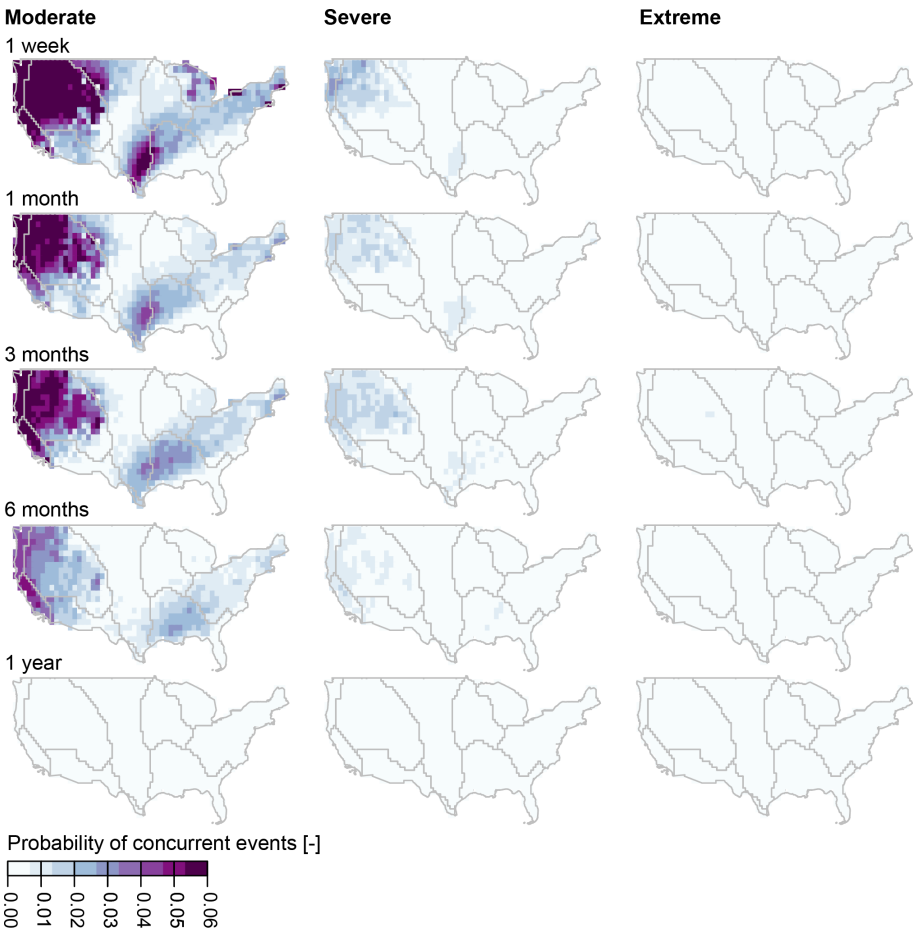

Figure 7. Probability of compound hot–dry events (number of compound events compared to the total number of months) at different timescales (1 week, 1 month, 3 months, 6 months, 1 year) and for three levels of extremeness (moderate $C_n > 0.8$, severe $C_n > 0.9$, and extreme $C_n > 0.95$) per grid cell. The darker the color, the higher the probability that a grid cell is affected by compound hot–dry events.

come small to nonexistent for extreme and long-lasting (i.e., annual) compound events.

The importance of T (STI) and P (SPI) as drivers of compound events varies by timescale and level of extremeness (Fig. 10). T is a particularly important driver at short timescales, as indicated by the high correlation between median STI and the median bivariate distribution of grid cells within a specific hydroclimatic region (Fig. 10a). The importance of P as a driver of compound events increases with timescale up to event durations of 6 months but decreases with level of extremeness (Fig. 10b). In summary, the longer the timescale, the more important P becomes as a driver compared to T (up to a seasonal timescale).

4 Discussion

The multi-site multi-variable stochastic model PRSim.weather proposed for the joint simulation of T and P at multiple sites has been shown to be suitable for the simulation of spatial multivariate hot–dry events. It reproduces the distributional and temporal autocorrelation characteristics of T and P at single sites, the dependence between the two variables, the spatial correlation of T and P across sites, and spatial patterns of STI, SPI, and their concurrence probabilities. However, spatial dependencies are slightly overestimated, while variable dependencies are slightly underestimated. The model still has acceptable performance across three types of dependencies – temporal, spatial, and variable – and enables studying rare spatial multivariate events, which would not be possible using observations only. Please note that even though the model generates yet unobserved observations, the simulations are not independent of the limited sample size used to fit the model because the model is data-driven like any other calibrated and/or fitted model. Please also note that while the model will be able to retain the statistical dependencies between variables to some degree, individual simulated events may not necessarily be physically consistent if many variables are jointly simulated. We note that stochastic approaches may be combined with physical approaches,

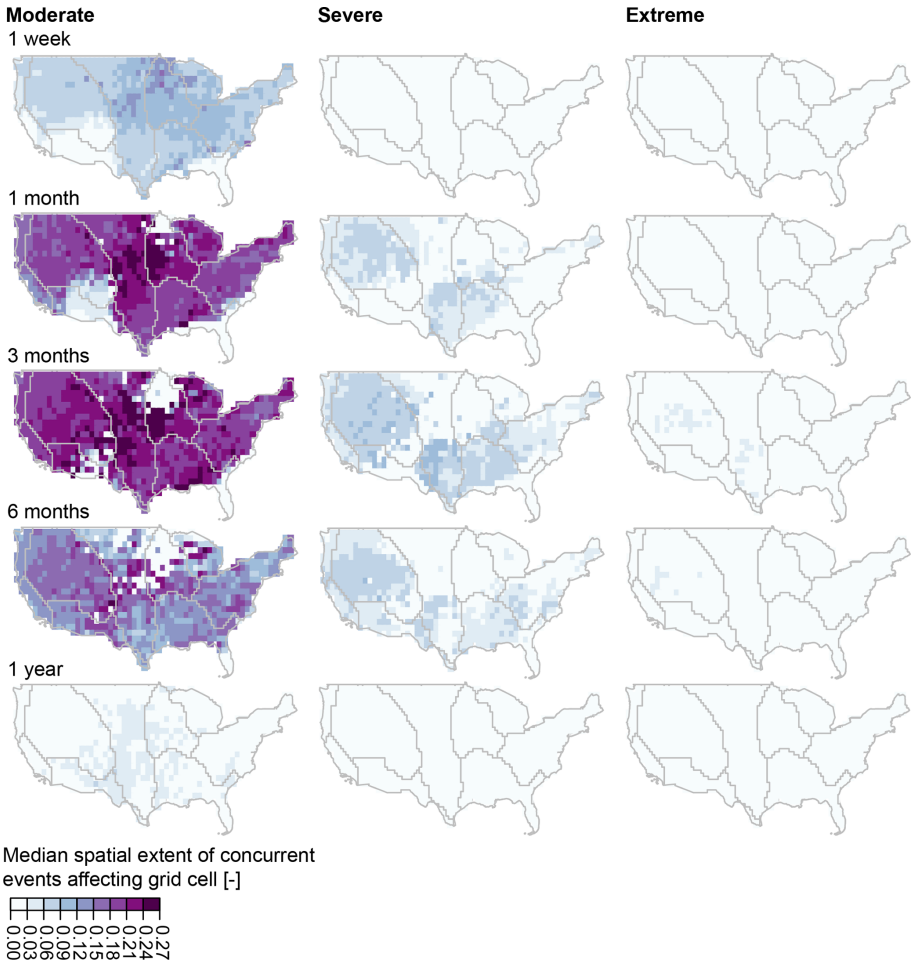

Figure 8. Spatial patterns of median compound event extent per grid cell for different timescales and extremeness levels over nine hydroclimatic regions. The darker the color, the higher the median spatial extent of compound events a grid cell is affected by.

such as in the weather generator AWE-GEN-2 by Peleg et al. (2017), or one may rely on large climate ensemble simulation approaches (Deser et al., 2020; Bevacqua et al., 2021).

Further model development should focus on how to improve the representation of dependencies in very high T–low P events at a daily scale and applications in other contexts as well as under nonstationary conditions. While the current application focuses on the two variables T and P in the US, the model can be adapted to other regions, other variables, and a multivariate context in which more than two variables are of interest. Adapting the model to other regions and variables requires reconsidering distribution choices, and extending it to a multivariate context necessitates adding more input variables, which are subsequently randomized in the same way as all other variables. Potential multivariate applications include the simulation of spatial concurrent pluvial, river, and coastal flooding by jointly modeling precipitation, discharge, and water levels or the joint simulation of wildfire drivers such as wind speed, temperature, and humidity. Extending model application to nonstationary conditions would require the implementation of nonstationary distributions for both T and P. For example, one could introduce covariates for certain parameters of the marginal distributions of T and P in Step 2 or introduce covariates with information about trends or variability in P and/or T to guide resampling in Step 4.

The finding that the western and southeastern US are most likely to be affected by compound hot–dry events at subannual timescales suggests that the likelihood of compound events is somehow related to precipitation seasonality, with regions receiving most of their precipitation in winter or spring and comparably less in summer and fall (Finkelstein and Truppi, 1991) being the most likely to be affected by compound events. In "normal" years, both the western and southeastern US receive a large part of their precipitation through recurrent patterns such as atmospheric rivers (Rutz et al., 2015) and tropical cyclones (Kunkel et al., 2012), respectively. Anomalies can arise because of temporal shifts or a weakening of these patterns in specific seasons and/or

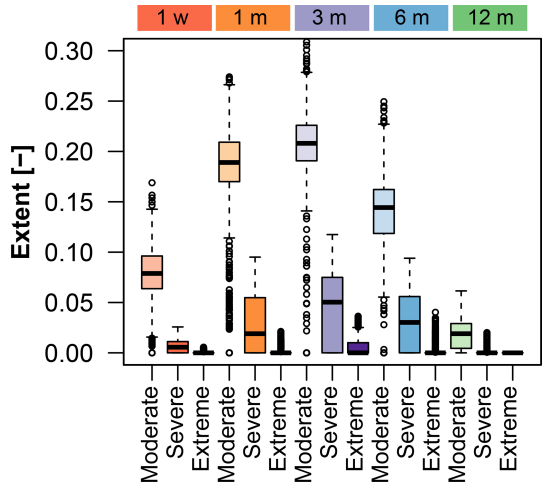

Figure 9. Relationship between compound event extent, timescale, and event extremeness. Box plots summarize the spread of median extent (percentage of overall area affected) across grid cells for weekly (red), monthly (orange), 3-monthly (purple), 6-monthly (blue), and annual (green) timescales and three levels of extremeness: moderate, severe, and extreme.

years. In addition, the regions most likely to experience compound events are the regions found to be most susceptible to heatwaves in the US (Smith et al., 2013).

Our finding that the spatial extents of compound events are largest for moderate events at sub-seasonal timescales implies that while these moderate events may have less severe impacts at a local scale, they may still be highly relevant at a regional scale. Compound events with large spatial extents represent a particular management challenge because they may preclude the transfer of resources and emergency supplies from one to another region. Consequently, the societal impacts of large-scale compound events can be amplified, since many coping strategies are predicated on some degree of resource transfer from less severely affected adjacent regions (Murgatroyd and Hall, 2020).

The finding that temperature is a comparably more important driver for short compound events only, while precipitation is comparably more important at seasonal timescales, corroborates the findings of previous studies about the importance of different hydrometeorological drivers at different timescales. Zhang et al. (2020) have shown that temperature is the most important hydrometeorological driver of short-term compound hot–dry extremes, which aligns with our findings. In addition, Tavakol et al. (2020) have shown that at long (i.e., annual) timescales, hot–dry–windy events co-occurred with major heatwaves, which is in line with our finding that temperature is an important driver of extreme compound hot–dry events at seasonal to annual timescales.

Future changes in the frequency and severity of compound hot–dry events are expected because of changes in both temperature and precipitation as well as their interdependence. The importance of temperature as a driver of short and extreme compound hot–dry events suggests that the increasing temperatures associated with climate change may induce future changes in the frequency and magnitude of short and extreme compound events. Such future increases have been projected globally (Wu et al., 2021) and regionally, e.g., for China (Zhou and Liu, 2018). In addition, previous studies have shown that the number and intensity of compound hot–dry events may increase because temperature and precipitation may become increasingly coupled and/or correlated in summer (De Luca et al., 2020; Zscheischler and Seneviratne, 2017), possibly as a consequence of an intensification of land–atmosphere feedbacks (Seneviratne et al., 2010). As the number of compound events increases locally, the area exposed to compound hot–dry events is projected to increase with global warming (Vogel et al., 2019), continuing a trend that has been already observed during the past few decades (Alizadeh et al., 2020). How exactly future changes in compound event extents relate to changes in drought spatial extent (Brunner et al., 2021) and in heatwave spatial extent remains to be investigated.

5 Summary and conclusions

We introduce the multi-variable multi-site stochastic model PRSim.weather to simulate continuous and spatially consistent multivariate time series. The model is shown to realistically simulate distributional and temporal autocorrelation characteristics of temperature and precipitation at single sites, dependencies between the two variables up to moderate extremes, spatial correlation patterns, and spatial heat and drought indicators as well as their co-occurrence probabilities for a gridded large-sample data set in the United States. However, future work is needed to improve the representation of very extreme hot–dry events. We apply the stochastic model to generate a large set of spatial and multivariate hot–dry events and use these simulated compound events to assess how event timescale and extremeness influence the spatial affectedness by compound hot–dry events over the United States, the spatial extent of compound events, and their main drivers temperature and precipitation. Our results show that (1) the northwest and southeast are most likely to be affected by compound hot–dry events independent of timescale; (2) the spatial extent of compound hot–dry events decreases with increasing event extremeness and timescale, i.e., the events with the largest spatial extents are typically short and only moderately extreme; and (3) temperature is an important driver of short compound events, while precipitation is an important driver at seasonal timescales, particularly for the moderately extreme events. These findings highlight the fact that occurrences of compound events are strongly influenced by the timescales at which they are defined. Research to quantify current compound event risk and to project it into the future will need to take timescale into

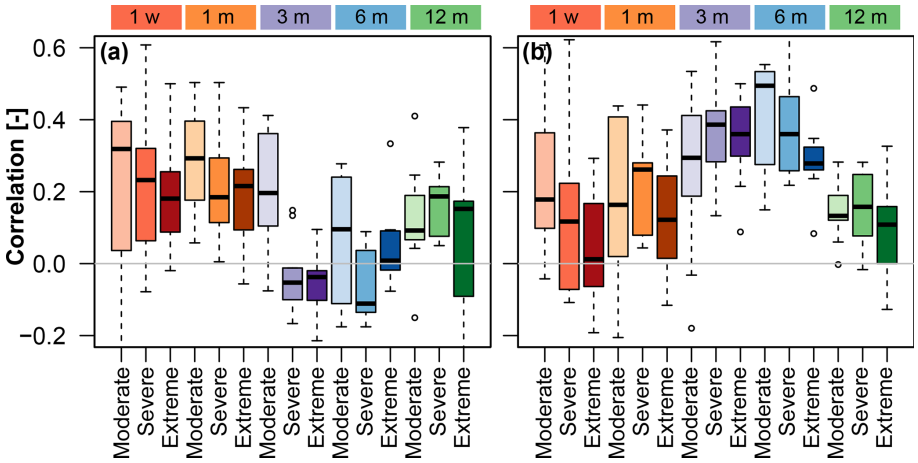

Figure 10. Importance of T and P as drivers of compound events across timescales and extremeness levels. Correlation of median bivariate distribution (empirical copula) per grid cell with median **(a)** STI and **(b)** SPI per grid cell. Correlations were computed using all simulation runs for nine hydroclimatic (Bukovsky) regions (spread of box plot) per timescale (color) and level of extremeness (hue).

consideration, especially as it also influences the sensitivity to different climate drivers and their potential future changes. Considering space scales and timescales in compound event assessments will allow us to make nuanced statements about which types of compound events may be changing because of increasing temperatures in a warming world. For example, short compound events and therefore events with large spatial extents may become more frequent with increasing temperatures, which will pose new regional management challenges.

Code and data availability. The ERA5-Land temperature and precipitation data used for this analysis can be downloaded from the Copernicus Climate Data Store: https://doi.org/10.24381/cds.e2161bac (ECMWF, 2019). The stochastic weather generator PRSim.weather is implemented in the R package PRSim under the function *PRSim.weather* and available for download at https://cran.r-project.org/web/packages/PRSim/ (last access: 12 January 2021) (Brunner and Furrer, 2019).

Author contributions. MIB developed the study concept and stochastic simulation model, performed all the analyses, and wrote the first draft of the paper. EG provided methodological advice and revised and edited the paper. AWW contributed to the interpretation of the results and revised and edited the paper.

Competing interests. The authors declare that they have no conflict of interest.

Special issue statement. This article is part of the special issue "Understanding compound weather and climate events and related impacts (BG/ESD/HESS/NHESS inter-journal SI)". It is not associated with a conference.

Acknowledgements. We would like to acknowledge high-performance computing support from Cheyenne (https://doi.org/10.5065/D6RX99HX) provided by NCAR's Computational and Information Systems Laboratory, sponsored by the National Science Foundation.

Financial support. This research has been supported by the Schweizerischer Nationalfonds zur Förderung der Wissenschaftlichen Forschung (grant no. P400P2_183844).

Review statement. This paper was edited by Jakob Zscheischler and reviewed by Emanuele Bevacqua and one anonymous referee.

References

Alizadeh, M. R., Adamowski, J., Nikoo, M. R., AghaKouchak, A., Dennison, P., and Sadegh, M.: A century of observations reveals increasing likelihood of continental-scale compound dry-hot extremes, Science Advances, 6, 1–12, https://doi.org/10.1126/sciadv.aaz4571, 2020.

Andreadis, K. M., Clark, E. A., Wood, A. W., Hamlet, A. F., and Lettenmaier, D. P.: Twentieth-century drought in the conterminous United States, J. Hydrometeorol., 6, 985–1001, https://doi.org/10.1175/JHM450.1, 2005.

Asquith, W.: lmomco: L-moments, censored L-moments, trimmed L-moments, L-comoments, and many distributions, available at: https://cran.r-project.org/web/packages/lmomco/index.html (last access: 12 January 2021), 2020.

Asquith, W. H.: Parameter estimation for the 4-parameter Asymmetric Exponential Power distribution by the method of L-moments using R, Comput. Stat. Data An., 71, 955–970, https://doi.org/10.1016/j.csda.2012.12.013, 2014.

Belzile, L., Wadsworth, J. L., Northrop, P. J., Grimshaw, S. D., Zhang, J., Stephens, M. A., Owen, A. B., and Huser, R.: R-package mev, available at: https://cran.r-project.org/web/packages/mev/index.html (last access: 12 January 2021), 2020.

Bevacqua, E., Shepherd, T. G., Watson, P. A. G., Sparrow, S., Wallom, D., and Mitchell, D.: Larger spatial footprint of wintertime total precipitation extremes in a warmer climate, Geophys. Res. Lett., 48, e2020GL091990, https://doi.org/10.1029/2020GL091990, 2021.

Bolós, V. J. and Benítez, R.: R-package wavScalogram, available at: https://cran.r-project.org/web/packages/wavScalogram/index.html (last access: 12 January 2021), 2020.

Brunner, M. I. and Furrer, R.: PRSim: Stochastic Simulation of Streamflow Time Series using Phase Randomization, available at: https://cran.r-project.org/web/packages/PRSim/ (last access: 12 January 2021), 2019.

Brunner, M. I. and Gilleland, E.: Stochastic simulation of streamflow and spatial extremes: a continuous, wavelet-based approach, Hydrol. Earth Syst. Sci., 24, 3967–3982, https://doi.org/10.5194/hess-24-3967-2020, 2020.

Brunner, M. I., Bárdossy, A., and Furrer, R.: Technical note: Stochastic simulation of streamflow time series using phase randomization, Hydrol. Earth Syst. Sci., 23, 3175–3187, https://doi.org/10.5194/hess-23-3175-2019, 2019.

Brunner, M. I., Swain, D. L., Gilleland, E., and Wood, A.: Increasing importance of temperature as a driver of streamflow drought spatial extent, Environ. Res. Lett., 16, 024038, https://doi.org/10.1088/1748-9326/abd2f0, 2021.

Bukovsky, M. S.: Masks for the Bukovsky regionalization of North America, available at: http://www.narccap.ucar.edu/contrib/bukovsky/ (last access: 8 May 2020), 2011.

Christian, J. I., Basara, J. B., Hunt, E. D., Otkin, J. A., and Xiao, S.: Flash drought development and cascading impacts associated with the 2010 Russian heatwave, Environ. Res. Lett., 15, 094078, https://doi.org/10.1088/1748-9326/ab9faf, 2020.

Cressie, N. A. C.: Statistics for spatial data, Wiley series in probability and mathematical statistics, John Wiley & Sons, Inc., Iowa State University, New York, 1993.

Deheuvels, P.: La fonction de dépendance empirique et ses propriétés. Un test non paramétrique d'indépendance, B. Cl. Sci. Ac. Roy. Belg., 65, 274–292, https://doi.org/10.3406/barb.1979.58521, 1979.

De Luca, P., Messori, G., Faranda, D., Ward, P. J., and Coumou, D.: Compound warm–dry and cold–wet events over the Mediterranean, Earth Syst. Dynam., 11, 793–805, https://doi.org/10.5194/esd-11-793-2020, 2020.

Deser, C., Lehner, F., Rodgers, K. B., Ault, T., Delworth, T. L., DiNezio, P. N., Fiore, A., Frankignoul, C., Fyfe, J. C., Horton, D. E., Kay, J. E., Knutti, R., Lovenduski, N. S., Marotzke, J., McKinnon, K. A., Minobe, S., Randerson, J., Screen, J. A., Simpson, I. R., and Ting, M.: Insights from Earth system model initial-condition large ensembles and future prospects, Nat. Clim. Change, 10, 277–286, https://doi.org/10.1038/s41558-020-0731-2, 2020.

Diederen, D., Liu, Y., Gouldby, B., Diermanse, F., and Vorogushyn, S.: Stochastic generation of spatially coherent river discharge peaks for continental event-based flood risk assessment, Nat. Hazards Earth Syst. Sci., 19, 1041–1053, https://doi.org/10.5194/nhess-19-1041-2019, 2019.

ECMWF: ERA5-Land hourly data from 1981 to present, Reading, UK, https://doi.org/10.24381/cds.e2161bac, 2019.

Evin, G., Favre, A.-C., and Hingray, B.: Stochastic generation of multi-site daily precipitation focusing on extreme events, Hydrol. Earth Syst. Sci., 22, 655–672, https://doi.org/10.5194/hess-22-655-2018, 2018.

Evin, G., Favre, A. C., and Hingray, B.: Stochastic generators of multi-site daily temperature: comparison of performances in various applications, Theor. Appl. Climatol., 135, 811–824, https://doi.org/10.1007/s00704-018-2404-x, 2019.

Feng, S., Wu, X., Hao, Z., Hao, Y., Zhang, X., and Hao, F.: A database for characteristics and variations of global compound dry and hot events, Weather and Climate Extremes, 30, 100299, https://doi.org/10.1016/j.wace.2020.100299, 2020.

Fernández, C. and Steel, M. F.: On bayesian modeling of fat tails and skewness, J. Am. Stat. Assoc., 93, 359–371, https://doi.org/10.1080/01621459.1998.10474117, 1998.

Finkelstein, P. L. and Truppi, L. E.: Spatial distribution of precipitation seasonality in the United States, J. Climate, 4, 373–385, 1991.

Fuchs, B. A., Wood, D. A., and Ebbeka, D.: From too much to too little. How the central U. S. drought of 2012 evolved out of one of the most devastating floods in record in 2011, Tech. rep., National Drought Mitigation Center, Lincoln, available at: https://digitalcommons.unl.edu/ndmcpub/5/ (last access: 15 November 2020), 2012.

Genest, C. and Favre, A.-C.: Everything you always wanted to know about copula modeling but were afraid to ask, J. Hydrol. Eng., 12, 347–367, https://doi.org/10.1061/(ASCE)1084-0699(2007)12:4(347), 2007.

Heffernan, J. E. and Tawn, J.: A conditional approach to modelling multivariate extreme values, J. R. Stat. Soc. B, 66, 497–546, https://doi.org/10.1111/j.1467-9868.2004.02050.x, 2004.

Hersbach, H., Bell, B., Berrisford, P., Hirahara, S., Horányi, A., Muñoz-Sabater, J., Nicolas, J., Peubey, C., Radu, R., Schepers, D., Simmons, A., Soci, C., Abdalla, S., Abellan, X., Balsamo, G., Bechtold, P., Biavati, G., Bidlot, J., Bonavita, M., Chiara, G., Dahlgren, P., Dee, D., Diamantakis, M., Dragani, R., Flemming, J., Forbes, R., Fuentes, M., Geer, A., Haimberger, L., Healy, S., Hogan, R. J., Hólm, E., Janisková, M., Keeley, S., Laloyaux, P., Lopez, P., Lupu, C., Radnoti, G., Rosnay, P., Rozum, I., Vamborg, F., Villaume, S., and Thépaut, J.: The ERA5 Global Reanalysis, Q. J. Roy. Meteor. Soc., 146, 1999–2049, https://doi.org/10.1002/qj.3803, 2020.

Keef, C., Tawn, J. A., and Lamb, R.: Estimating the probability of widespread flood events, Environmetrics, 24, 13–21, https://doi.org/10.1002/env.2190, 2013.

Kunkel, K. E., Easterling, D. R., Kristovich, D. A. R., Gleason, B., Stoecker, L., and Smith, R.: Meteorological causes of the secular variations in observed extreme precipitation events for the conterminous United States, J. Hydrometeorol., 13, 1131–1141, https://doi.org/10.1175/JHM-D-11-0108.1, 2012.

Lancaster, G., Iatsenko, D., Pidde, A., Ticcinelli, V., and Stefanovska, A.: Surrogate data for hypothesis testing of physical systems, Phys. Rep., 748, 1–60, https://doi.org/10.1016/j.physrep.2018.06.001, 2018.

Manning, C., Widmann, M., Bevacqua, E., Van Loon, A. F., Maraun, D., and Vrac, M.: Increased probability of compound long-duration dry and hot events in Europe during summer (1950-2013), Environ. Res. Lett., 14, 094006, https://doi.org/10.1088/1748-9326/ab23bf, 2019.

Mazdiyasni, O. and AghaKouchak, A.: Substantial increase in concurrent droughts and heatwaves in the United States, P. Natl. Acad. Sci. USA, 112, 11484–11489, https://doi.org/10.1073/pnas.1422945112, 2015.

McKee, T. B., Doesken, N. J., and Kleist, J.: The relationship of drought frequency and duration to time scales, in: Proceedings of the 8th Conference on Applied Climatology, American Meteorological Society, January, Anaheim, California, available at: https://www.droughtmanagement.info/literature/AMS_Relationship_Drought_Frequency_Duration_Time_Scales_1993.pdf (last access: 15 November 2020), 1993.

Mo, K. C. and Lettenmaier, D. P.: Heat wave flash droughts in decline, Geophys. Res. Lett., 42, 2823–2829, https://doi.org/10.1002/2015GL064018, 2015.

Murgatroyd, A. and Hall, J. W.: The resilience of interbasin transfers to severe droughts with changing spatial characteristics, Front. Environ. Sci., 8, 571647, https://doi.org/10.3389/fenvs.2020.571647, 2020.

Naveau, P., Huser, R., Ribereau, P., and Hannart, A.: Modeling jointly low, moderate, and heavy rainfall intensities without a threshold selection, Water Resour. Res., 52, 2753–2769, https://doi.org/10.1002/2015WR018552, 2016.

Papastathopoulos, I. and Tawn, J. A.: Extended generalised Pareto models for tail estimation, J. Stat. Plan. Infer., 143, 131–143, https://doi.org/10.1016/j.jspi.2012.07.001, 2013.

Peleg, N., Fatichi, S., Paschalis, A., Molnar, P., and Burlando, P.: An advanced stochastic weather generator for simulating 2-D high-resolution climate variables, J. Adv. Model. Earth Sy., 9, 1595–1627, https://doi.org/10.1002/2013MS000282, 2017.

Rajagopalan, B., Salas, J. D., and Lall, U.: Stochastic methods for modeling precipitation and streamflow, chap. 2, in: Advances in data-based approaches for hydrologic modeling and forecasting, edited by: Sivakumar, B. and Berndtsson, R., World Scientific, New Jersey, 17–52, 2010.

Rutz, J. J., James Steenburgh, W., and Martin Ralph, F.: The inland penetration of atmospheric rivers over western North America: A Lagrangian analysis, Mon. Weather Rev., 143, 1924–1944, https://doi.org/10.1175/MWR-D-14-00288.1, 2015.

Sarhadi, A., Ausín, M. C., Wiper, M. P., Touma, D., and Diffenbaugh, N. S.: Multidimensional risk in a nonstationary climate: Joint probability of increasingly severe warm and dry conditions, Science Advances, 4, eaau3487, https://doi.org/10.1126/sciadv.aau3487, 2018.

Schreiber, T. and Schmitz, A.: Surrogate time series, Physica D, 142, 346–382, https://doi.org/10.1016/S0167-2789(00)00043-9, 2000.

Seneviratne, S. I., Corti, T., Davin, E. L., Hirschi, M., Jaeger, E. B., Lehner, I., Orlowsky, B., and Teuling, A. J.: Investigating soil moisture-climate interactions in a changing climate: A review, Earth-Sci. Rev., 99, 125–161, https://doi.org/10.1016/j.earscirev.2010.02.004, 2010.

Smith, T. T., Zaitchik, B. F., and Gohlke, J. M.: Heat waves in the United States: definitions, patterns and trends, Climatic Change, 118, 811–825, https://doi.org/10.1007/s10584-012-0659-2, 2013.

Stedinger, J. R. and Taylor, M. R.: Synthetic streamflow generation. 1. Model verification and validation, Water Resour. Res., 18, 909–918, 1982.

Tavakol, A., Rahmani, V., and Harrington, J.: Temporal and spatial variations in the frequency of compound hot, dry, and windy events in the central United States, Sci. Rep.-UK, 10, 1–13, https://doi.org/10.1038/s41598-020-72624-0, 2020.

Torrence, C. and Compo, G. P.: A practical guide to wavelet analysis, B. Am. Meteorol. Soc., 79, 61–78, 1998.

Vogel, M. M., Zscheischler, J., Wartenburger, R., Dee, D., and Seneviratne, S. I.: Concurrent 2018 hot extremes across northern hemisphere due to human-induced climate change, Earths Future, 7, 692–703, https://doi.org/10.1029/2019EF001189, 2019.

Vogel, R. M. and Stedinger, J. R.: The value of stochastic streamflow models in overyear reservoir design applications, Water Resour. Res., 24, 1483–1490, https://doi.org/10.1029/WR024i009p01483, 1988.

Wegren, S.: Food security and Russia's 2010 drought, Eurasian Geogr. Econ., 52, 140–156, https://doi.org/10.2747/1539-7216.52.1.140, 2011.

Wu, J., Chen, X., Yu, Z., Yao, H., Li, W., and Zhang, D.: Assessing the impact of human regulations on hydrological drought development and recovery based on a 'simulated-observed' comparison of the SWAT model, J. Hydrol., 577, 123990, https://doi.org/10.1016/j.jhydrol.2019.123990, 2019.

Wu, X., Hao, Z., Tang, Q., Singh, V. P., Zhang, X., and Hao, F.: Projected increase in compound dry and hot events over global land areas, Int. J. Climatol., 41, 393–403, https://doi.org/10.1002/joc.6626, 2021.

Yu, R. and Zhai, P.: More frequent and widespread persistent compound drought and heat event observed in China, Sci. Rep.-UK, 10, 1–7, https://doi.org/10.1038/s41598-020-71312-3, 2020.

Zhang, H., Wu, C., Yeh, P. J., and Hu, B. X.: Global pattern of short-term concurrent hot and dry extremes and its relationship to large-scale climate indices, Int. J. Climatol., 40, 5906–5924, https://doi.org/10.1002/joc.6555, 2020.

Zhou, P. and Liu, Z.: Likelihood of concurrent climate extremes and variations over China, Environ. Res. Lett., 13, 094 023, https://doi.org/10.1088/1748-9326/aade9e, 2018.

Zscheischler, J. and Seneviratne, S. I.: Dependence of drivers affects risks associated with compound events, Science Advances, 3, 1–11, https://doi.org/10.1126/sciadv.1700263, 2017.

Zscheischler, J., Michalak, A. M., Schwalm, C., Mahecha, M. D., Huntzinger, D. N., Reichstein, M., Berthier, G., Ciais, P., Cook, R. B., El-Masri, B., Huang, M., Ito, A., Jain, A., King, A., Lei, H., Lu, C., Mao, J., Peng, S., Poulter, B., Ricciuto, D., Shi, X., Tao, B., Tian, H., Viovy, N., Wang, W., Wei, Y., Yang, J., and Zeng, N.: Impact of large-scale climate extremes on biospheric carbon fluxes: An intercomparison

based on MsTMIP data, Global Biogeochem. Cy., 28, 585–600, https://doi.org/10.1002/2014GB004826, 2014.

Zscheischler, J., Westra, S., Hurk, B. J. J. M. V. D., Seneviratne, S. I., Ward, P. J., Pitman, A., Aghakouchak, A., Bresch, D. N., and Leonard, M.: Future climate risk from compound events, Nat. Clim. Change, 8, 469–477, https://doi.org/10.1038/s41558-018-0156-3, 2018.

Zscheischler, J., Martius, O., Westra, S., Bevacqua, E., Raymond, C., Horton, R. M., Hurk, B. v. d., AghaKouchak, A., Jezequel, A., Mahecha, M. D., Maraun, D., Ramos, A. M., Ridder, N. N., Thiery, W., and Vignotto, E.: A typology of compound weather and climate events, Nature Reviews Earth & Environment, 1, 333–347, https://doi.org/10.1038/s43017-020-0060-z, 2020.